
EQUIVARIANT OBSERVER DESIGN ON $SL(3)$ FOR IMAGE INTENSITY-BASED HOMOGRAPHY ESTIMATION

PREPRINT*

 **Tarek Bouazza**

I3S, CNRS, Université Côte d'Azur
06900 Sophia Antipolis, France
bouazza@i3s.unice.fr

 **Pieter van Goor**

School of Aerospace, Mechanical, and
Mechatronic Engineering (AMME)
Faculty of Engineering, University of Sydney
NSW, 2006, Australia
pieter.vangoor@sydney.edu.au

 **Robert Mahony**

Systems Theory and Robotics Group
Australian National University
ACT, 2601, Australia
Robert.Mahony@anu.edu.au

 **Tarek Hamel**

I3S, CNRS, Université Côte d'Azur
and Institut Universitaire de France (IUF)
06900 Sophia Antipolis, France
thamel@i3s.unice.fr

May 12, 2026

ABSTRACT

This paper addresses the problem of homography estimation using a nonlinear observer designed on the Lie group $SL(3)$ that exploits the full image information through direct image registration. Unlike traditional feature-based methods, which rely on extensive feature extraction and matching, the proposed approach formulates an observer that minimises a cost function defined directly in terms of image pixel intensities. Explicit conditions ensuring the non-degeneracy of the cost function are derived, and a comprehensive analysis is conducted to characterise and generate degenerate (unobservable) image configurations. Theoretical results demonstrate local exponential convergence of the observer. To improve local convergence properties, a second-order observer variant is introduced by incorporating the Hessian of the cost function into the correction term. Simulation results demonstrate the performance of the proposed solutions on real images.

1 Introduction

Advances in exteroceptive sensors, such as high-resolution cameras, LiDAR and RGB-D devices, have enabled autonomous systems to capture detailed information about their environment. Exploiting this information is critical for applications such as Simultaneous Localisation and Mapping (SLAM) [Forster et al., 2014] and 3D reconstruction [Geiger et al., 2011]. Directly estimating rigid-body motion and geometric transformations from raw measurements presents a promising alternative to traditional landmark- or feature-based methods, which rely on extracting and matching sparse keypoints and can fail in environments where features are scarce or affected by noise. Dense methods exploit the full information available across the sensor domain, such as pixel intensities, optical flow fields, or dense depth maps to achieve more robust and accurate estimation [Forster et al., 2014, Kerl et al., 2013]. A prominent example is the computation of the *homography* matrix, which describes the relative transformation between two camera views of a planar surface [Hartley and Zisserman, 2003].

Homography estimation has been widely studied in the computer vision, computer graphics, and robotics communities. Traditional techniques extract a sparse set of salient features, such as points, lines, conics and contours, to perform feature matching and then compute a homography estimate by solving algebraic constraints or optimisation problems over individual frames or a set of selected images [Kaminski and Shashua, 2004, Agarwal et al., 2005]. One widely used method is the Direct Linear Transform (DLT) algorithm [Hartley and Zisserman, 2003], which computes the homography from at least four point

*Under review

correspondences by solving a linear system via Singular Value Decomposition (SVD). Direct (or intensity-based) methods, on the other hand, estimate homographies using raw image pixel intensities without explicit feature extraction or matching [Szeliski et al., 2007]. They generally outperform feature-based methods in situations where feature detection is difficult or images lack distinctive features. However, direct methods typically have a limited convergence range and require complex optimisation techniques and higher computational cost to efficiently process the entire image data, especially for high-resolution images. Classical direct approaches formulate the problem as an image registration (or alignment) task [Shum and Szeliski, 1998], which aims to find the homography parameters that minimise a photometric cost between a reference and a target image, and optimise a cost function based on pixel intensity differences between images. Common cost functions include the sum of squared differences [Baker and Matthews, 2004, Benhimane and Malis, 2004] and the normalised cross-correlation [Szeliski et al., 2007]. The resulting optimisation problems are solved iteratively using algorithms such as steepest-descent, Gauss-Newton, and Levenberg-Marquardt [Baker and Matthews, 2004, Szeliski and Kang, 1995]. A seminal method is the Lucas-Kanade algorithm [Lucas and Kanade, 1981], which updates the homography parameters iteratively to minimize intensity differences. The forward compositional algorithm [Shum and Szeliski, 2002] improves this approach by estimating an incremental warp rather than an additive increment, while the inverse compositional method [Baker and Matthews, 2004] further improves efficiency by reversing the roles of reference and target images, allowing pre-computation of the inverse Hessian and steepest descent images. The efficient second-order minimization (ESM) method [Benhimane and Malis, 2004] approximates the Hessian to achieve faster convergence and a larger convergence domain.

In recent years, significant work has been dedicated to designing nonlinear observers for the estimation of homographies with dynamics. A number of successful approaches have exploited the $\mathbf{SL}(3)$ Lie group structure of the set of homographies [Benhimane and Malis, 2007] to yield powerful stability guarantees [Mahony et al., 2012, Hamel et al., 2011, Hua et al., 2019, 2020]. By exploiting the temporal correlations and velocity information inherent to robotics problems, these methods outperform algorithms that process each image independently. Hamel et al. [2011] proposed a nonlinear deterministic observer on $\mathbf{SL}(3)$ using point-feature correspondences built upon Lyapunov-based design principles. Later, Hua et al. [2019] extended this line of work by developing a recursive observer from the general theory of gradient-based nonlinear observers for kinematic systems with equivariant outputs [Mahony et al., 2013]. Further extensions of the framework in [Mahony et al., 2013] incorporated richer feature modalities. For instance, image line and point-feature correspondences were combined in [Hua et al., 2020] for computing the innovation term, while Hua et al. [2017] considered conic-feature correspondences such as ellipses and hyperbolas. Beyond deterministic designs, Bernal et al. [2023] formulated a Bayesian filtering framework on $\mathbf{SL}(3)$, and derived both an iterative EKF and an interacting multiple model (IMM) filter to estimate the homography using point-feature correspondences. More recently, an equivariant filter (EqF) was proposed by the authors in [Bouazza et al., 2023a] to estimate homography from rigid-body velocity measurements and point-feature correspondences.

This paper build on the authors' prior work on intensity-based homography estimation on $\mathbf{SL}(3)$ [Bouazza et al., 2023b] and proposes a new class of nonlinear observers that directly exploit the photometric information contained in image data. The approach is based on the natural group action of $\mathbf{SL}(3)$ on the sphere \mathbb{S}^2 and its induced action on the Sobolev space of weakly twice differentiable square-integrable functions $W^{2,2}(\mathbb{S}^2)$. Images are modelled as functions warped by an evolving homography, and a photometric cost function is defined through this group action. A nonlinear observer on $\mathbf{SL}(3)$ is then designed to minimise this cost and estimate the dynamic homography. The main contributions are:

1. We show that the action of $\mathbf{SL}(3)$ on the sphere \mathbb{S}^2 induces an action of $\mathbf{SL}(3)$ on $W^{2,2}(\mathbb{S}^2)$ and exploit this to define a direct photometric cost function for homography estimation from raw image intensities. We then derive a gradient-based observer on $\mathbf{SL}(3)$ to minimise this cost.
2. We perform an observability analysis and identify a local non-degeneracy condition characterised by the stabilizer subgroup of the reference image under $\mathbf{SL}(3)$, and illustrate degenerate cases with unobservable image configurations.
3. We prove global stability and local exponential convergence of the observer under the derived non-degeneracy condition and introduce a variant that scales the correction by the inverse Hessian of the cost function to improve convergence.
4. We present simulation results on real images to validate the convergence of the proposed observers.

The remainder of the paper is organised as follows. Section 2 introduces the necessary preliminaries on square-integrable functions on the sphere and the special linear group $\mathbf{SL}(3)$. Section 3 formulates the homography estimation problem and presents a detailed observability analysis in the dense image intensity measurement setting, where observability conditions are established. Section 4 derives the dense observer on $\mathbf{SL}(3)$, including the gradient-based and second-order variants to improve convergence. Section 5 presents simulation results on real image sequences to demonstrate the effectiveness and robustness of the proposed observer. Finally, Section 6 concludes the paper and discusses directions for future research.

2 Preliminary material

2.1 Notation

We denote by \mathbb{R} and $\mathbb{R}_{\geq 0}$ the sets of real and nonnegative real numbers, respectively. The n -dimensional Euclidean space is denoted by \mathbb{R}^n . We denote by $\mathbb{R}^{m \times n}$ the set of real $m \times n$ matrices. The set of $n \times n$ symmetric positive definite matrices is denoted by $\mathbb{S}_+(n)$, and the identity matrix is denoted by $I_n \in \mathbb{R}^{n \times n}$. For any matrix $K \in \mathbb{S}_+(n)$, we define the K -weighted inner product of two vectors $x, y \in \mathbb{R}^n$ by $\langle x, y \rangle_K := x^\top K y$ and the associated norm as $|x|_K := \sqrt{x^\top K x}$. For $K = I_n$, they reduce to the standard Euclidean inner product and norm,

$$\langle x, y \rangle := x^\top y \quad |x| := \sqrt{x^\top x}. \quad (1)$$

Given $a \in \mathbb{R}^3$, let a^\times denote the skew-symmetric matrix associated with the vector (cross) product, which satisfies $a^\times b = a \times b$ for all $a, b \in \mathbb{R}^3$.

For matrices $A, B \in \mathbb{R}^{n \times n}$, the Euclidean matrix inner product and associated Frobenius norm are defined as

$$\langle A, B \rangle := \text{tr}(A^\top B), \quad |A| := \sqrt{\langle A, A \rangle}. \quad (2)$$

Any square matrix $A \in \mathbb{R}^{3 \times 3}$ admits the decomposition $A = \mathbb{P}_s(A) + \mathbb{P}_a(A)$, where the symmetric and skew-symmetric components are defined by

$$\mathbb{P}_s(A) := \frac{1}{2}(A + A^\top), \quad \mathbb{P}_a(A) := \frac{1}{2}(A - A^\top).$$

2.2 Square-integrable functions on embedded manifolds

Given a smooth manifold \mathcal{M} , $T_{\mathbf{x}}\mathcal{M}$ denotes the tangent space at $\mathbf{x} \in \mathcal{M}$, and $\mathfrak{X}(\mathcal{M})$ the set of smooth vector fields on \mathcal{M} . Given $f : \mathcal{M} \rightarrow \mathcal{N}$ and $g : \mathcal{N} \rightarrow \mathcal{N}'$, their composition is denoted by $g \circ f : \mathcal{M} \rightarrow \mathcal{N}'$, where $(g \circ f)(\mathbf{x}) = g(f(\mathbf{x}))$.

Let $\mathbb{S}^2 := \{\mathbf{x} \in \mathbb{R}^3 \mid |\mathbf{x}| = 1\} \subset \mathbb{R}^3$ be the 2-dimensional unit sphere with the Riemannian metric induced by the Euclidean inner product in \mathbb{R}^3 . For any point $\mathbf{x} \in \mathbb{S}^2$, the tangent space is $T_{\mathbf{x}}\mathbb{S}^2 := \{u \in \mathbb{R}^3 \mid \langle u, \mathbf{x} \rangle = 0\}$. A convenient choice of local coordinates on \mathbb{S}^2 is given by the spherical parametrization $(\theta, \phi) \in [0, \pi] \times [0, 2\pi)$, where $\mathbf{x}(\theta, \phi) = (\sin \theta \cos \phi, \sin \theta \sin \phi, \cos \theta)^\top$. In these coordinates, the associated area element (Riemannian volume form) is $dV_g = \sin \theta d\theta d\phi$, which is the standard surface area element on \mathbb{S}^2 . For any $\mathbf{x} \in \mathbb{S}^2$, the orthogonal projection onto $T_{\mathbf{x}}\mathbb{S}^2$ is defined by

$$\pi_{\mathbf{x}} := I_3 - \mathbf{x}\mathbf{x}^\top.$$

A square-integrable function on \mathbb{S}^2 is a real-valued map $f : \mathbb{S}^2 \rightarrow \mathbb{R}$ such that

$$\|f\|^2 := \int_{\mathbb{S}^2} |f(\mathbf{x})|^2 dV_g$$

exists and is finite. The space of all square-integrable functions on \mathbb{S}^2 is denoted $\mathbb{L}^2(\mathbb{S}^2)$, and is a Hilbert space; that is, a real vector space equipped with an inner product defined by

$$\langle f, h \rangle := \int_{\mathbb{S}^2} f(\mathbf{x})h(\mathbf{x})dV_g, \quad \forall f, h \in \mathbb{L}^2(\mathbb{S}^2).$$

We denote by ∇ the Levi-Civita connection on \mathbb{S}^2 . The covariant derivative of a tangent vector field $X \in \mathfrak{X}(\mathbb{S}^2)$ along $u \in T_{\mathbf{x}}\mathbb{S}^2$ is defined by projecting the usual Euclidean derivative to the tangent space $\nabla_u X := \pi_{\mathbf{x}}(D\tilde{X}(\mathbf{x})[u])$, where \tilde{X} is any smooth extension of X to a neighborhood of \mathbf{x} in \mathbb{R}^3 .

For a smooth function $f : \mathbb{S}^2 \rightarrow \mathbb{R}$, the covariant derivative along $u \in T_{\mathbf{x}}\mathbb{S}^2$ coincides with the directional derivative

$$\nabla_u f = Df(\mathbf{x})[u] = \left. \frac{d}{dt} \right|_{t=0} f(\gamma(t)),$$

for any smooth curve γ with $\gamma(0) = \mathbf{x}$, $\dot{\gamma}(0) = u$. The gradient ∇f satisfies

$$\nabla_u f = \langle \nabla f(\mathbf{x}), u \rangle, \quad \forall u \in T_{\mathbf{x}}\mathbb{S}^2,$$

and is given by $\nabla f(\mathbf{x}) = \pi_{\mathbf{x}} \nabla_{\mathbb{R}^3} f(\mathbf{x})$. The Hessian is

$$\nabla^2 f(\mathbf{x})[u, v] := \langle \nabla_u \nabla f, v \rangle, \quad \forall u, v \in T_{\mathbf{x}}\mathbb{S}^2.$$

Definition 1 (Weak derivative on \mathbb{S}^2 , [Chan and Czubak, 2024]). *A function $f : \mathbb{S}^2 \rightarrow \mathbb{R}$ is said to admit a weak k -th order covariant derivative, $k \geq 1$, if there exists a covariant k -tensor field $\tilde{\nabla}^k f$ such that*

$$\int_{\mathbb{S}^2} f(\mathbf{x}) \nabla^k \phi(\mathbf{x}) dV_g = (-1)^k \int_{\mathbb{S}^2} \langle \tilde{\nabla}^k f(\mathbf{x}), \phi(\mathbf{x}) \rangle dV_g$$

for all smooth, compactly supported k -tensor fields ϕ on \mathbb{S}^2 . In particular, $\tilde{\nabla} f$ denotes the weak gradient and $\tilde{\nabla}^2 f$ is the weak Hessian of f .

Definition 2 (Sobolev space, [Hebey, 1996]). *The Sobolev space $W^{k,2}(\mathbb{S}^2)$ is defined as*

$$W^{k,2}(\mathbb{S}^2) := \{f : \mathbb{S}^2 \rightarrow \mathbb{R} \mid f, \tilde{\nabla}^l f \in \mathbb{L}^2(\mathbb{S}^2), \forall l = 1, \dots, k\}.$$

This space consists of all functions in $\mathbb{L}^2(\mathbb{S}^2)$ whose weak derivatives up to order k are also square-integrable.

When f is smooth on an open set in \mathbb{S}^2 , the weak derivatives coincide with the classical ones almost everywhere on this set, i.e., $\tilde{\nabla} f = \nabla f$, $\tilde{\nabla}^2 f = \nabla^2 f$. The weak derivatives, however, are still well-defined even if f fails to be differentiable on a set of measure-zero in \mathbb{S}^2 (e.g., at isolated points or along curves).

2.3 Special Linear Group $\mathbf{SL}(3)$

For a detailed introduction to matrix Lie groups, the reader is referred to [Baker, 2003].

A *matrix Lie group* \mathbf{G} is a subgroup of the general linear group $\mathbf{GL}(n) := \{A \in \mathbb{R}^{n \times n} \mid \det(A) \neq 0\}$ closed under matrix multiplication and inversion. Its Lie algebra is the linear space identified with the tangent space at the identity, $\mathfrak{g} := \mathbb{T}_{I_n} \mathbf{G} \subset \mathbb{R}^{n \times n}$. The exponential map $\exp : \mathfrak{g} \rightarrow \mathbf{G}$ defines a local diffeomorphism from a neighbourhood of $0 \in \mathfrak{g}$ to a neighbourhood of $I_n \in \mathbf{G}$.

The inner product (2) naturally induces a right-invariant Riemannian metric on \mathbf{G} via

$$\langle U_1 X, U_2 X \rangle_X := \langle U_1, U_2 \rangle, \quad U_1, U_2 \in \mathfrak{g}, \quad X \in \mathbf{G}.$$

The special orthogonal group $\mathbf{SO}(3)$ of three-dimensional rotations and its Lie algebra $\mathfrak{so}(3)$ are defined by

$$\begin{aligned} \mathbf{SO}(3) &:= \{R \in \mathbb{R}^{3 \times 3} \mid \det(R) = 1, RR^\top = R^\top R = I_3\}, \\ \mathfrak{so}(3) &:= \{\Omega^\times \in \mathbb{R}^{3 \times 3} \mid \Omega \in \mathbb{R}^3\}. \end{aligned}$$

The special linear group $\mathbf{SL}(3)$ of matrices with unit determinant and its Lie algebra $\mathfrak{sl}(3)$ are defined by

$$\begin{aligned} \mathbf{SL}(3) &:= \{H \in \mathbb{R}^{3 \times 3} \mid \det(H) = 1\}, \\ \mathfrak{sl}(3) &:= \{U \in \mathbb{R}^{3 \times 3} \mid \text{tr}(U) = 0\}. \end{aligned}$$

The projection $\mathbb{P}_{\mathbf{SL}(3)} : \mathbb{R}^{3 \times 3} \rightarrow \mathbf{SL}(3)$ for any non-singular matrix $H \in \mathbb{R}^{3 \times 3}$ is defined as

$$\mathbb{P}_{\mathbf{SL}(3)}(H) := \det(H)^{-\frac{1}{3}} H \in \mathbf{SL}(3). \quad (3)$$

Let $\{e_1, e_2, e_3\}$ denote the canonical basis of \mathbb{R}^3 , and let $\{B_j\}_{j=1}^8$ be the following orthonormal basis of $\mathfrak{sl}(3)$ with respect to the Frobenius inner product:

$$\begin{aligned} B_1 &= \frac{1}{\sqrt{2}}(e_1 e_1^\top - e_2 e_2^\top), & B_2 &= \frac{1}{\sqrt{2}}(e_1 e_2^\top + e_2 e_1^\top), \\ B_3 &= \frac{1}{\sqrt{2}}(e_1 e_3^\top + e_3 e_1^\top), & B_4 &= \frac{1}{\sqrt{2}}(e_2 e_3^\top + e_3 e_2^\top), \\ B_5 &= \frac{1}{\sqrt{2}}(e_1 e_2^\top - e_2 e_1^\top), & B_6 &= \frac{1}{\sqrt{2}}(e_1 e_3^\top - e_3 e_1^\top), \\ B_7 &= \frac{1}{\sqrt{2}}(e_2 e_3^\top - e_3 e_2^\top), & B_8 &= \frac{1}{\sqrt{6}}(e_1 e_1^\top + e_2 e_2^\top - 2e_3 e_3^\top). \end{aligned}$$

The *wedge operator* $(\cdot)^\wedge : \mathbb{R}^8 \rightarrow \mathfrak{sl}(3)$ is the linear isomorphism defined by $v^\wedge := \sum_{j=1}^8 v_j B_j$, for $v \in \mathbb{R}^8$. The *vec* $(\cdot)^\vee : \mathfrak{sl}(3) \rightarrow \mathbb{R}^8$ denotes its inverse, given by $V^\vee := (\langle V, B_1 \rangle, \dots, \langle V, B_8 \rangle)^\top$, $V \in \mathfrak{sl}(3)$.

A right action of $\mathbf{SL}(3)$ on the sphere \mathbb{S}^2 is a smooth map $\rho : \mathbf{SL}(3) \times \mathbb{S}^2 \rightarrow \mathbb{S}^2$ that satisfies the *identity* and *compatibility* properties:

$$\rho(I_3, \mathbf{y}) = \mathbf{y}, \quad \rho(G, \rho(H, \mathbf{y})) = \rho(HG, \mathbf{y}),$$

for any $H, G \in \mathbf{SL}(3)$, $\mathbf{y} \in \mathbb{S}^2$. The map $\rho_H : \mathbb{S}^2 \rightarrow \mathbb{S}^2$, for any fixed $H \in \mathbf{SL}(3)$, is a diffeomorphism $\rho_H(\mathbf{y}) := \rho(H, \mathbf{y})$. Likewise, for any fixed $\mathbf{y} \in \mathbb{S}^2$, $\rho_{\mathbf{y}} : \mathbf{SL}(3) \rightarrow \mathbb{S}^2$ defines a smooth projection $\rho_{\mathbf{y}}(H) := \rho(H, \mathbf{y})$.

2.4 Homographies as elements of the special linear group $\mathbf{SL}(3)$

Consider a camera moving in space while observing a stationary planar scene. As it moves, the camera captures images of the scene from different viewpoints. Let $\{\mathring{\mathcal{C}}\}$ denote the reference camera frame, associated with the viewpoint at a fixed initial time, and let $\{\mathcal{C}_t\}$ denote the current camera frame at time t .

Let $R \in \mathbf{SO}(3)$ and $\xi \in \mathbb{R}^3$ denote the orientation and position, respectively, of the frame $\{\mathcal{C}_t\}$ with respect to the reference frame $\{\mathring{\mathcal{C}}\}$. Let d denote the distance from the origin of $\{\mathcal{C}_t\}$ to the planar scene and $\eta \in \mathbb{S}^2$ the normal vector pointing to the scene expressed in $\{\mathcal{C}_t\}$. The plane is defined by $\mathbf{\Pi} := \{P \in \mathbb{R}^3 \mid \eta^\top P - d = 0\}$. Let $\mathring{P} \in \{\mathring{\mathcal{C}}\}$ and $P \in \{\mathcal{C}_t\}$ be the 3D coordinate vectors of a point belonging to the scene, related by

$$\mathring{P} = RP + \xi. \quad (4)$$

Under the pinhole model [Ma et al., 2004], the intrinsic camera parameters, such as the focal length and the principal point, are captured by a calibration matrix $K \in \mathbb{R}^{3 \times 3}$, such that the projection of a point \mathring{P} (resp. P) onto the image plane is $\mathring{\zeta} = K\mathring{P}$ (resp. $\zeta = KP$). The image homography $H_{im} \in \mathbb{R}^{3 \times 3}$ that maps pixel coordinates from $\{\mathcal{C}_t\}$ to $\{\mathring{\mathcal{C}}\}$ is given by

$$H_{im} := \gamma K \left(R + \frac{\xi \eta^\top}{d} \right) K^{-1},$$

where $\gamma > 0$ is an unknown scale factor. The corresponding *Euclidean homography* $H \in \mathbb{R}^{3 \times 3}$ is

$$H := K^{-1}H_{im}K = \gamma \left(R + \frac{\xi \eta^\top}{d} \right). \quad (5)$$

The scale factor γ can be chosen to ensure that $\det(H) = 1$, i.e., to set $H = \mathbb{P}_{\mathbf{SL}(3)}(R + \xi \eta^\top / d)$. This corresponds to taking $\gamma := \det(R + \xi \eta^\top / d)^{-\frac{1}{3}} = (d/\mathring{d})^{\frac{1}{3}}$ (see [Mahony et al., 2012]). For the remainder of this paper, all homographies H are taken to be appropriately scaled to satisfy $H \in \mathbf{SL}(3)$.

We model image maps as real-valued functions defined on the sphere $I : \mathbb{S}^2 \rightarrow [0, 1]$. That is, instead of using pixel coordinates on the image plane, intensity values are defined at points represented by the ray directions $\mathbf{x} \in \mathbb{S}^2$, corresponding to a spherical perspective projection model. We will use this formulation in the remainder of the paper, as working on the sphere adds to the clarity of the mathematical presentation.

Proposition 1 ([Hua et al., 2020]). *The mapping $\rho : \mathbf{SL}(3) \times \mathbb{S}^2 \rightarrow \mathbb{S}^2$ given by*

$$\rho(H, \mathbf{x}) := \frac{H^{-1}\mathbf{x}}{|H^{-1}\mathbf{x}|}, \quad (6)$$

is a right group action of $\mathbf{SL}(3)$ on \mathbb{S}^2 .

Assumption 1. *The observed planar surface is Lambertian, i.e., it reflects light uniformly in all directions.*

Assumption 1 corresponds to the classical *brightness constancy* constraint used in direct image alignment methods [Irani and Anandan, 1999]. It postulates that the radiance of a given scene point remains constant across different viewpoints. As a consequence, if \mathbf{x} and $\rho_H(\mathbf{x})$ denote corresponding bearing vectors in two images related by a homography action ρ_H , then the measured intensities along these directions satisfy $I_1(\mathbf{x}) = I_2(\rho_H(\mathbf{x}))$.

Assumption 2. *All image maps I are assumed to be square-integrable and twice weakly differentiable in $\mathbb{L}^2(\mathbb{S}^2)$, i.e., they belong to the Sobolev space $W^{2,2}(\mathbb{S}^2)$.*

The assumption of square-integrability of image maps is justified by the fact that real-world images have bounded pixel intensity values and are defined on the compact domain \mathbb{S}^2 . Modelling image maps in the Sobolev space $W^{2,2}(\mathbb{S}^2)$ further accounts for non-smooth images, such as those with edges or intensity discontinuities, by only requiring the existence of weak derivatives rather than strict pointwise differentiability of the image maps.

Under Assumptions 1 and 2, the action ρ defined in (6) induces a natural right group action of $\mathbf{SL}(3)$ on image maps in $W^{2,2}(\mathbb{S}^2)$, as established in the following lemma.

Lemma 1. *The mapping $\mu : \mathbf{SL}(3) \times W^{2,2}(\mathbb{S}^2) \rightarrow W^{2,2}(\mathbb{S}^2)$, defined by*

$$\mu(H, I) := I \circ \rho_{H^{-1}}, \quad (7)$$

is a right group action.

Proof. Checking the identity property, for any $I \in W^{2,2}(\mathbb{S}^2)$ and $\mathbf{x} \in \mathbb{S}^2$,

$$\boldsymbol{\mu}(I_3, I)(\mathbf{x}) = I \circ \boldsymbol{\rho}_{I_3}(\mathbf{x}) = I(\mathbf{x}).$$

Now checking the composition property, for any $I \in W^{2,2}(\mathbb{S}^2)$, any $\mathbf{x} \in \mathbb{S}^2$, and any $G, H \in \mathbf{SL}(3)$, one has

$$\begin{aligned} \boldsymbol{\mu}(G, \boldsymbol{\mu}(H, I)) &= \boldsymbol{\mu}(G, I \circ \boldsymbol{\rho}_{H^{-1}}), \\ &= I \circ \boldsymbol{\rho}_{H^{-1}} \circ \boldsymbol{\rho}_{G^{-1}}, \\ &= I \circ \boldsymbol{\rho}_{G^{-1}H^{-1}}, \\ &= I \circ \boldsymbol{\rho}_{(HG)^{-1}} = \boldsymbol{\mu}(HG, I). \end{aligned}$$

Finally, we show that $W^{2,2}(\mathbb{S}^2)$ is closed under the action $\boldsymbol{\mu}$, i.e., that $\boldsymbol{\mu}(H, I) \in W^{2,2}(\mathbb{S}^2)$ for all $I \in W^{2,2}(\mathbb{S}^2)$ and fixed $H \in \mathbf{SL}(3)$. Recall that $I \in W^{2,2}(\mathbb{S}^2)$ implies $I \in \mathbb{L}^2(\mathbb{S}^2)$ with $\tilde{\nabla}I, \tilde{\nabla}^2I \in \mathbb{L}^2(\mathbb{S}^2)$. We begin by showing that $\boldsymbol{\mu}(H, I) \in \mathbb{L}^2(\mathbb{S}^2)$. Since $H \in \mathbf{SL}(3)$ is fixed, the map $\boldsymbol{\rho}_H : \mathbb{S}^2 \rightarrow \mathbb{S}^2$ is a smooth diffeomorphism. By definition, $\boldsymbol{\mu}(H, I)(\mathbf{x}) = I(\boldsymbol{\rho}_{H^{-1}}(\mathbf{x}))$. Using the change of variables $\mathbf{y} = \boldsymbol{\rho}_{H^{-1}}(\mathbf{x})$, we obtain

$$\begin{aligned} \|\boldsymbol{\mu}(H, I)\|^2 &= \int_{\mathbb{S}^2} I(\boldsymbol{\rho}_{H^{-1}}(\mathbf{x}))^2 dV_g(\mathbf{x}) \\ &= \int_{\mathbb{S}^2} I(\mathbf{y})^2 |\det(D\boldsymbol{\rho}_H(\mathbf{y}))| dV_g(\mathbf{y}). \end{aligned}$$

The differential of $\boldsymbol{\rho}_H$ is given by

$$D\boldsymbol{\rho}_H(\mathbf{y}) = \frac{1}{|H^{-1}\mathbf{y}|} \pi_{\boldsymbol{\rho}_H(\mathbf{y})} H^{-1}. \quad (8)$$

For any orthonormal basis (v_1, v_2) of $T_{\mathbf{y}}\mathbb{S}^2$, the Jacobian determinant satisfies

$$|\det D\boldsymbol{\rho}_H(\mathbf{y})| = |(D\boldsymbol{\rho}_H(\mathbf{y})v_1) \times (D\boldsymbol{\rho}_H(\mathbf{y})v_2)| = \frac{|H^\top \mathbf{y}|}{|H^{-1}\mathbf{y}|^3}.$$

This expression is continuous and strictly positive on the compact manifold \mathbb{S}^2 . Therefore, there exists a constant $M_0(H) > 0$ such that $|\det(D\boldsymbol{\rho}_H(\mathbf{y}))| \leq M_0(H)$, for all $\mathbf{y} \in \mathbb{S}^2$. It follows that

$$\|\boldsymbol{\mu}(H, I)\|^2 \leq M_0(H) \|I\|^2 < \infty,$$

and hence $\boldsymbol{\mu}(H, I) \in \mathbb{L}^2(\mathbb{S}^2)$.

We now consider the first covariant derivative. We have $\tilde{\nabla}\boldsymbol{\mu}(H, I)(\mathbf{x}) = D\boldsymbol{\rho}_{H^{-1}}(\mathbf{x})^\top (\tilde{\nabla}I)(\boldsymbol{\rho}_{H^{-1}}(\mathbf{x}))$. Using again the change of variables $\mathbf{y} = \boldsymbol{\rho}_{H^{-1}}(\mathbf{x})$, we obtain

$$\begin{aligned} \|\tilde{\nabla}\boldsymbol{\mu}(H, I)\|^2 &= \int_{\mathbb{S}^2} |D\boldsymbol{\rho}_{H^{-1}}(\boldsymbol{\rho}_H(\mathbf{y}))^\top (\tilde{\nabla}I)(\mathbf{y})|^2 |\det(D\boldsymbol{\rho}_H(\mathbf{y}))| dV_g(\mathbf{y}). \end{aligned}$$

Since $\boldsymbol{\rho}_H$ is a smooth diffeomorphism and H is fixed, both $D\boldsymbol{\rho}_{H^{-1}}$ and $|\det(D\boldsymbol{\rho}_H)|$ are continuous and bounded on \mathbb{S}^2 . Therefore, there exists a constant $M_1(H) > 0$ such that

$$\|\tilde{\nabla}\boldsymbol{\mu}(H, I)\|^2 \leq M_1(H) \|\tilde{\nabla}I\|^2 < \infty.$$

Finally, we consider the second covariant derivative. A direct computation yields

$$\begin{aligned} \tilde{\nabla}^2\boldsymbol{\mu}(H, I)(\mathbf{x})[u, v] &= \tilde{\nabla}_u(\tilde{\nabla}\boldsymbol{\mu}(H, I))[v] \\ &= D\boldsymbol{\rho}_{H^{-1}}(\mathbf{x})^\top (\tilde{\nabla}^2I)(\boldsymbol{\rho}_{H^{-1}}(\mathbf{x})) D\boldsymbol{\rho}_{H^{-1}}(\mathbf{x})[u, v] \\ &\quad + \sum_{i=1}^2 (\tilde{\nabla}I)(\boldsymbol{\rho}_{H^{-1}}(\mathbf{x})) \cdot (\tilde{\nabla}_u D\boldsymbol{\rho}_{H^{-1}}(\mathbf{x})[v]), \end{aligned}$$

Since $\boldsymbol{\rho}_{H^{-1}}$ is smooth and \mathbb{S}^2 is compact, both $D\boldsymbol{\rho}_{H^{-1}}$ and its covariant derivative $\tilde{\nabla}D\boldsymbol{\rho}_{H^{-1}}$ are bounded. Consequently, there exists a constant $M_2(H) > 0$ such that

$$\|\tilde{\nabla}^2\boldsymbol{\mu}(H, I)\|^2 \leq M_2(H) (\|\tilde{\nabla}^2I\|^2 + \|\tilde{\nabla}I\|^2) < \infty.$$

Since $I \in W^{2,2}(\mathbb{S}^2)$ implies that $I, \tilde{\nabla}I$, and $\tilde{\nabla}^2I$ all belong to $\mathbb{L}^2(\mathbb{S}^2)$, we conclude that $\boldsymbol{\mu}(H, I) \in W^{2,2}(\mathbb{S}^2)$. Therefore, $W^{2,2}(\mathbb{S}^2)$ is closed under the action of $\boldsymbol{\mu}$. This completes the proof. \square

Remark 1. Despite $\boldsymbol{\mu}$ being defined on $W^{2,2}(\mathbb{S}^2)$, the output space of interest is the orbit of a fixed image map I under homography transformations, given by

$$\text{orb}_{\boldsymbol{\mu}}(I) := \{I \circ \boldsymbol{\rho}_{H^{-1}} \mid H \in \mathbf{SL}(3)\} \subset W^{2,2}(\mathbb{S}^2).$$

3 Application to homography estimation

Consider a camera that is moving according to some measured linear and angular velocity while capturing images of a planar scene. Let $H(t) \in \mathbf{SL}(3)$ denote the homography that maps the current image to a fixed reference image, with left-invariant kinematics given by

$$\dot{H} = HU, \quad (9)$$

where $U \in \mathfrak{sl}(3)$ is the group velocity derived from the camera motion. We consider the case where the group velocity is fully measured.

Assumption 3. *The group velocity $U \in \mathfrak{sl}(3)$ is available from measurements.*

3.1 Homography Observer Design

Let $\hat{H} \in \mathbf{SL}(3)$ denote the estimate of H , and define the dynamics of the proposed observer to be

$$\dot{\hat{H}} = \hat{H}U + \Delta\hat{H}, \quad \hat{H}(0) = I_3, \quad (10)$$

where $\Delta \in \mathfrak{sl}(3)$ denotes the correction term that remains to be designed.

Define the group error $E := \hat{H}H^{-1}$, its dynamics are

$$\dot{E} = \hat{H}UH^{-1} + \Delta H\hat{H}^{-1} - \hat{H}UH^{-1} = \Delta E. \quad (11)$$

The problem of the observer design is to identify a correction term $\Delta \in \mathfrak{sl}(3)$ that ensures that the group error E converges to the identity I_3 , and therefore

$$\hat{H} = \hat{H}H^{-1}H = EH \rightarrow I_3H = H.$$

In what follows, the correction term Δ is obtained from the gradient descent direction of a suitable non-degenerate cost function. This is conceptually similar to the designs based on image feature measurements [Hua et al., 2019, 2020], with the key difference that here the cost function is constructed directly from raw image intensities.

We define the reference image as a map $\mathring{I} : \mathcal{X} \rightarrow [0, 1]$, $\mathring{I} \in W^{2,2}(\mathcal{X})$, where $\mathcal{X} := \text{dom}(\mathring{I}) \subset \mathbb{S}^2$ denotes the fixed reference image domain, corresponding to the projection of a planar surface patch onto the spherical image surface. Although \mathcal{X} may represent only a subset of the full image, we refer to \mathring{I} as the *reference image* throughout the estimation problem, since all computations are performed on this fixed domain.

Assuming the scene is planar, the current image map can be expressed in terms of the homography H as

$$\begin{aligned} I &:= \boldsymbol{\mu}(H, \mathring{I}), \\ I(\mathbf{x}) &= \boldsymbol{\mu}(H, \mathring{I})(\mathbf{x}) = \mathring{I}(\boldsymbol{\rho}(H^{-1}, \mathbf{x})). \end{aligned}$$

Using a homography estimate \hat{H} , we define the *warped image* (or error image) map by exploiting the group action property of $\boldsymbol{\mu}$:

$$I^e := \boldsymbol{\mu}(\hat{H}^{-1}, I) = I \circ \boldsymbol{\rho}_{\hat{H}} = \mathring{I} \circ \boldsymbol{\rho}_E = \boldsymbol{\mu}(E^{-1}, \mathring{I}). \quad (12)$$

The map I^e therefore provides a direct measure of the estimation error in the image space, such that $I^e = \mathring{I}$ if $E = I_3$ (i.e., $\hat{H} = H$).

Using the estimate \hat{H} and pixel intensity information of the reference and current images, we introduce a *photometric* cost function $\mathcal{C} : \mathbf{SL}(3) \times W^{2,2}(\mathcal{X}) \rightarrow \mathbb{R}_{\geq 0}$ associated with the observer (10), defined as

$$\begin{aligned} \mathcal{C}(\hat{H}, I) &:= \frac{1}{2} \|I^e - \mathring{I}\|^2, \\ &= \frac{1}{2} \int_{\mathcal{X}} \left(\boldsymbol{\mu}(\hat{H}^{-1}, I)(\mathbf{x}) - \mathring{I}(\mathbf{x}) \right)^2 dV_g. \end{aligned} \quad (13)$$

Remark 2. *The warped image map (12) is defined on the time-varying domain $\text{dom}(\boldsymbol{\mu}(\hat{H}(t)^{-1}, I))$ that depends on the current homography estimate $\hat{H}(t)$. To ensure that the cost (14) can be evaluated over the entire fixed domain \mathcal{X} , the map I^e is restricted to the intersection $\mathcal{X}^e := \mathcal{X} \cap \text{dom}(\boldsymbol{\mu}(\hat{H}(t)^{-1}, I))$, and extended by zero on $\mathcal{X} \setminus \mathcal{X}^e$. Although this extension may introduce a jump discontinuity across the boundary $\partial\mathcal{X}^e$, the cost (14) remains well-defined since the image maps are elements of the Sobolev space $W^{2,2}(\mathcal{X})$.*

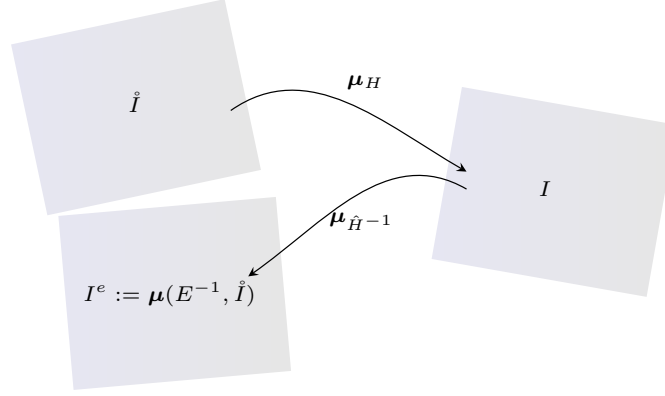


Figure 1: In the image space, the transformation μ_H parameterises image I in terms of the reference image \hat{I} , so the $\mu_{\hat{H}^{-1}}$ transformation generates a warped (error) image, which converges to the reference image when $\hat{H} \rightarrow H$.

Since $I, \hat{I} \in W^{2,2}(\mathcal{X})$, the cost (13) is well-defined and differentiable in the weak sense. Additionally, exploiting the definition of the warped image, it can be equivalently expressed in terms of the homography error E as

$$\mathcal{C}(E, \hat{I}) = \frac{1}{2} \int_{\mathcal{X}} \left(\mu(E^{-1}, \hat{I})(\mathbf{x}) - \hat{I}(\mathbf{x}) \right)^2 dV_g. \quad (14)$$

More generally, the cost (13) is *right-invariant* in the sense that $\mathcal{C}(\phi(Q, \hat{H}), \mu(Q, I)) = \mathcal{C}(\hat{H}, I)$ for all $Q \in \mathbf{SL}(3)$. This property is particularly convenient because it allows all subsequent computations to be parameterised purely in terms of E . Since \hat{I} is constant, the evolution of (14) is driven fully by the error system (11).

Local convergence of the observer error requires the cost to be non-degenerate. The following lemma provides a necessary condition for \mathcal{C} to satisfy this property.

Lemma 2. *Suppose that the image maps \hat{I} and I are twice weakly differentiable and let $\tilde{\nabla} \hat{I}(\mathbf{x})$ denote the reference image map gradient at \mathbf{x} . If there exists a measurable subset $\mathcal{U} \subset \mathcal{X}$ of strictly positive measure such that*

$$\int_{\mathcal{U}} \left\langle \tilde{\nabla} \hat{I}(\mathbf{x}) \mathbf{x}^\top, \Delta \right\rangle^2 dV_g(\mathbf{x}) > 0, \quad (15)$$

then the cost function (14) has an isolated global minimum at $E = I_3$.

Proof. It is straightforward to see that $\mathcal{C}(I_3, \hat{I}) = 0$ and is therefore a global minimum. To show that this is an isolated minimum, it suffices to show that the Hessian of \mathcal{C} at the identity I_3 is non-degenerate. The first order derivative of \mathcal{C} is computed as follows,

$$\begin{aligned} D_1 \mathcal{C}(E, \hat{I})[\Delta E] &= \int_{\mathcal{X}} \left(I^e(\mathbf{x}) - \hat{I}(\mathbf{x}) \right) D(\hat{I} \circ \rho_{\mathbf{x}})(E)[\Delta E] dV_g \\ &= \int_{\mathcal{X}} \left(I^e(\mathbf{x}) - \hat{I}(\mathbf{x}) \right) \left. \frac{d}{dt} \hat{I} \circ \rho(\exp(t\Delta)E, \mathbf{x}) \right|_{t=0} dV_g \\ &= \int_{\mathcal{X}} \left(I^e(\mathbf{x}) - \hat{I}(\mathbf{x}) \right) \left. \frac{d}{dt} \hat{I} \circ \rho(E, \rho(\exp(t\Delta), \mathbf{x})) \right|_{t=0} dV_g \\ &= \int_{\mathcal{X}} \left(I^e(\mathbf{x}) - \hat{I}(\mathbf{x}) \right) \left. \frac{d}{dt} I^e \circ \rho(\exp(t\Delta), \mathbf{x}) \right|_{t=0} dV_g \\ &= \int_{\mathcal{X}} \left(I^e(\mathbf{x}) - \hat{I}(\mathbf{x}) \right) \tilde{D} I^e(\mathbf{x}) D \rho_{\mathbf{x}}(I_3)[\Delta] dV_g. \end{aligned}$$

where $\tilde{D}I^e(\mathbf{x})$ denotes the transpose of the warped image weak gradient at \mathbf{x} ; that is, $\tilde{D}I^e(\mathbf{x}) = \tilde{\nabla}I^e(\mathbf{x})^\top$. The differential $D\rho_{\mathbf{x}}(I_3)[\Delta]$ is given by

$$\begin{aligned} D\rho_{\mathbf{x}}(I_3)[\Delta] &= \left. \frac{d}{dt} \right|_{t=0} \rho(\exp(t\Delta), \mathbf{x}), \\ &= \frac{1}{|\mathbf{x}|^2} \left(-\Delta\mathbf{x}|\mathbf{x}| + \frac{\mathbf{x}\mathbf{x}^\top \Delta\mathbf{x}}{|\mathbf{x}|} \right), \\ &= (\mathbf{x}\mathbf{x}^\top - I_3) \Delta\mathbf{x} = -\pi_{\mathbf{x}}\Delta\mathbf{x}, \end{aligned} \quad (16)$$

and since $\tilde{D}\dot{I}(\mathbf{x})\pi_{\mathbf{x}} = \tilde{D}\dot{I}(\mathbf{x})$, it follows

$$D_1\mathcal{C}(E, \dot{I})[\Delta E] = - \int_{\mathcal{X}} \left(I^e(\mathbf{x}) - \dot{I}(\mathbf{x}) \right) \tilde{D}I^e(\mathbf{x}) \Delta\mathbf{x} dV_g.$$

Now, the second order derivative of \mathcal{C} about I_3 is

$$\begin{aligned} D_1^2\mathcal{C}(I_3, \dot{I})[\Delta, \Delta] &= - \int_{\mathcal{X}} \left(D(\dot{I} \circ \rho_{\mathbf{x}})(E)[\Delta E] \right) \tilde{D}I^e(\mathbf{x}) \Delta\mathbf{x} dV_g \\ &\quad - \int_{\mathcal{X}} \left(I^e(\mathbf{x}) - \dot{I}(\mathbf{x}) \right) \left. \frac{d}{dt} (\tilde{D}I^e(\mathbf{x}) \Delta\mathbf{x}) dV_g \right|_{E=I_3}, \\ &= - \int_{\mathcal{X}} \left(\tilde{D}\dot{I}(\mathbf{x}) D\rho_{\mathbf{x}}(I_3)[\Delta] \right) \tilde{D}\dot{I}(\mathbf{x}) \Delta\mathbf{x} dV_g, \\ &= \int_{\mathcal{X}} \left(\tilde{D}\dot{I}(\mathbf{x}) \Delta\mathbf{x} \right)^2 dV_g, \end{aligned}$$

and, hence

$$\begin{aligned} D_1^2\mathcal{C}(I_3, \dot{I})[\Delta, \Delta] &= \int_{\mathcal{X}} \left(\text{tr}(\tilde{D}\dot{I}(\mathbf{x}) \Delta\mathbf{x}) \right)^2 dV_g, \\ &= \int_{\mathcal{X}} \left(\text{tr}(\mathbf{x} \tilde{D}\dot{I}(\mathbf{x}) \Delta) \right)^2 dV_g, \\ &= \int_{\mathcal{X}} \left\langle \tilde{\nabla}\dot{I}(\mathbf{x})\mathbf{x}^\top, \Delta \right\rangle^2 dV_g. \end{aligned} \quad (17)$$

Observe that $\text{grad}\dot{I}(\mathbf{x})\mathbf{x}^\top \in \mathfrak{sl}(3)$ as $\text{tr}(\text{grad}\dot{I}(\mathbf{x})\mathbf{x}^\top) = \text{tr}(\tilde{D}\dot{I}(\mathbf{x})\mathbf{x}) = 0$. Now suppose the Hessian is degenerate; i.e. there exists a non-zero $\Delta \in \mathfrak{sl}(3)$ such that $D_1^2\mathcal{C}(I_3, \dot{I})[\Delta, \Delta] = 0$. Then, since the integrand in (17) is non-negative for every \mathbf{x} and $\tilde{\nabla}\dot{I}$ exists almost everywhere on \mathcal{X} , it must be that

$$\left\langle \tilde{\nabla}\dot{I}(\mathbf{x})\mathbf{x}^\top, \Delta \right\rangle = 0, \quad (18)$$

for almost every $\mathbf{x} \in \mathcal{X}$. This implies that for any subset $\mathcal{U} \subseteq \mathcal{X}$ of positive measure,

$$\int_{\mathcal{U}} \left\langle \tilde{\nabla}\dot{I}(\mathbf{x})\mathbf{x}^\top, \Delta \right\rangle^2 dV_g = 0.$$

That is, $\left\langle \tilde{\nabla}\dot{I}(\mathbf{x})\mathbf{x}^\top, \Delta \right\rangle$ vanishes almost everywhere on \mathcal{U} . This contradicts the assumption (15), and therefore the Hessian (17) must be non-degenerate, and the cost has an isolated global minimum at $E = I_3$. \square

Lemma 3. *The non-degeneracy condition (15) holds if and only if the stabilizer*

$$\text{stab}_{\mu}(\dot{I}) := \{E \in \mathbf{SL}(3) \mid \dot{I} \circ \rho_E \simeq \dot{I}\}, \quad (19)$$

is discrete, where, given $I_1, I_2 \in W^{2,2}(\mathcal{X})$, we define $I_1 \simeq I_2$ to mean that $I_1(\mathbf{x}) = I_2(\mathbf{x})$ for almost all $\mathbf{x} \in \mathcal{X}$. Equivalently, the kernel of the differential

$$\ker D\mu_{\dot{I}}(I_3) := \{\Delta \in \mathfrak{sl}(3) \mid D\mu_{\dot{I}}(I_3)[\Delta] \simeq 0\} = \mathfrak{sl}(3),$$

where we write $D\mu_{\dot{I}}(I_3)[\Delta] \simeq 0$ to mean that $D\mu_{\dot{I}}(I_3)(\mathbf{x}) = 0$ for almost all $\mathbf{x} \in \mathcal{X}$.

Proof. The relation (18) can be equivalently expressed as $\langle \tilde{\nabla} \dot{I}(\mathbf{x}), \pi_{\mathbf{x}} \Delta \mathbf{x} \rangle = 0$, and hence

$$\left\langle D\rho_{\mathbf{x}}(I_3)[\Delta], \tilde{\nabla} \dot{I}(\mathbf{x}) \right\rangle = 0, \quad (20)$$

for almost every $\mathbf{x} \in \mathcal{X}$. If this holds for all $\Delta \in (3)$, then it is exactly the kernel condition in the lemma statement.

To see that this implies the stabilizer condition (19), suppose there exists a non-zero $\Delta \in \mathfrak{sl}(3)$ satisfying (20). Then \dot{I} remains invariant almost everywhere along the flow lines generated by $t \mapsto \rho(\exp(t\Delta), \mathbf{x})$ for all $t \in \mathbb{R}$. Specifically, one has

$$\begin{aligned} & \frac{d}{dt} \frac{1}{2} \int_{\mathcal{X}} |\dot{I} \circ \rho_{\exp(t\Delta)}(\mathbf{x}) - \dot{I}(\mathbf{x})|^2 dV_g \\ &= \int_{\mathcal{X}} \left\langle \dot{I} \circ \rho_{\exp(t\Delta)}(\mathbf{x}) - \dot{I}(\mathbf{x}), \tilde{D}\dot{I}(\rho_{\exp(t\Delta)}(\mathbf{x})) D\rho_{\rho_{\exp(t\Delta)}(\mathbf{x})}(I_3)[\Delta] \right\rangle dV_g \\ &= \int_{\mathcal{X}} \langle \dot{I} \circ \rho_{\exp(t\Delta)}(\mathbf{x}) - \dot{I}(\mathbf{x}), 0 \rangle dV_g = 0. \end{aligned}$$

It follows that $\dot{I} \circ \rho_{\exp(t\Delta)}(\mathbf{x}) = \dot{I}(\mathbf{x})$ for almost all \mathbf{x} for all $t \in \mathbb{R}$. Thus, $\exp(t\Delta)$ lies in the stabilizer subgroup $\text{stab}_{\mu}(\dot{I})$, which is therefore continuous. Conversely, this also shows that if $\text{stab}_{\mu}(\dot{I})$ is continuous, then there exists a nonzero $\Delta \in \text{stab}_{\mu}(\dot{I})$ in its Lie algebra that satisfies (18). \square

Remark 3. *The standard non-degeneracy condition in observer design based on feature measurements (see Mahony et al. [2013]) requires a finite set of measured features $(\hat{y}_1, \dots, \hat{y}_n)$ to satisfy $\bigcap_{i=1}^n \text{stab}_{\rho}(\hat{y}_i) = \{I_3\}$. Condition (19) can be viewed as a continuous counterpart that extends this requirement to intensity-based measurements modelled as maps in the Sobolev space $W^{2,2}(\mathcal{X})$.*

3.2 Generation of degenerate images

Degeneracies in the cost arise when the reference image admits continuous symmetries captured by its stabilizer subgroup. To illustrate situations in which condition (19) is violated, we construct reference images with intrinsic continuous symmetries. That is, each reference image \dot{I} is constructed such that $\dot{I}(\rho(\exp(t\Delta), \mathbf{x})) = \dot{I}(\mathbf{x})$ for all $t \in \mathbb{R}$ and $\mathbf{x} \in \mathcal{X}$, for some $\Delta \in \mathfrak{sl}(3)$ generating a one-parameter subgroup $\{\exp(t\Delta)\} \subset \text{stab}_{\mu}(\dot{I})$.

We numerically synthesise such images by sampling a set of points in \mathcal{X} and propagating them along their orbits induced by the corresponding group action for multiple values of t . The procedure is implemented in Python, and we generate six reference images, shown in Fig. 2. Each image is invariant under the flow of a specific one-parameter subgroup of $\mathbf{SL}(3)$, generated by an element $\Delta \in \mathfrak{sl}(3)$ inducing a continuous projective transformation of the image.

4 Gradient-based observer derivation

The cost function defined in (14) can be viewed as a candidate Lyapunov function for the observer design, where the correction term can be obtained directly from its gradient flow, as outlined in the following theorem.

Theorem 1. *Consider the kinematics (9) and assume that the group velocity $U \in \mathfrak{sl}(3)$ is known. Consider the observer (10) and the cost function \mathcal{C} defined by (14) and suppose that the cost is non-degenerate in the sense of Lemma 2. Define the correction term*

$$\Delta = k_{\Delta} \int_{\mathcal{X}} r(\mathbf{x}) \tilde{\nabla} I^e(\mathbf{x}) \mathbf{x}^{\top} dV_g, \quad (21)$$

where $r(\mathbf{x}) = I^e(\mathbf{x}) - \dot{I}(\mathbf{x})$ denotes the image intensity residual at \mathbf{x} and $k_{\Delta} > 0$ a chosen gain. Then, its time derivative satisfies $\dot{\mathcal{C}}(E) = -|\Delta|^2/k_{\Delta}$, and the equilibrium $E = I_3$ of the autonomous system (11) is locally exponentially stable.

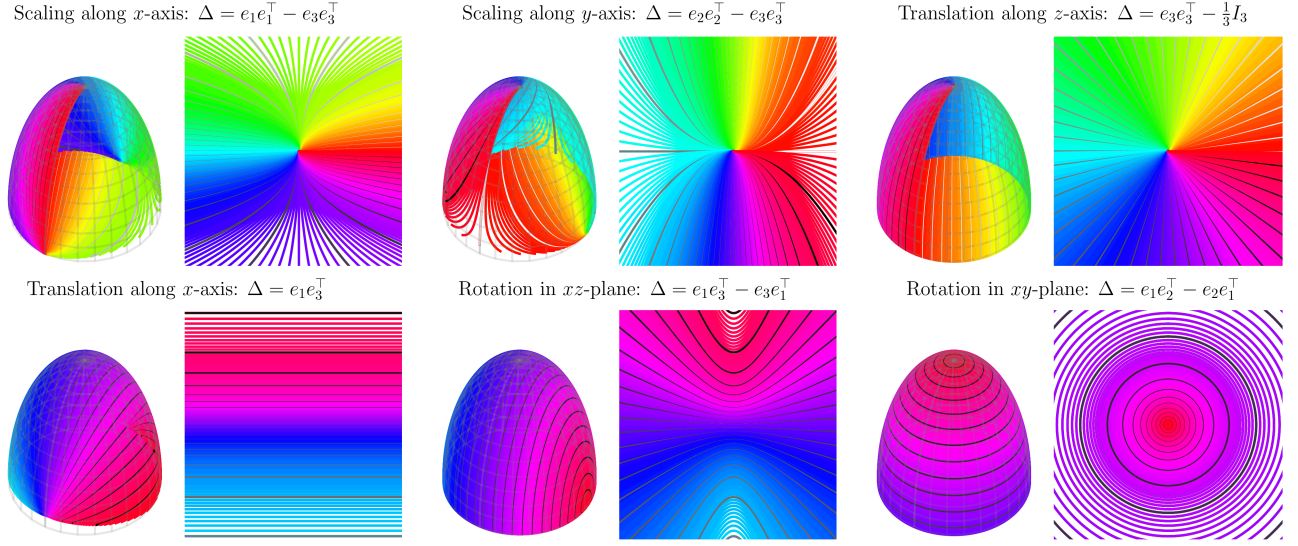


Figure 2: Numerically constructed degenerate reference images exhibiting continuous symmetries invariant under one-parameter subgroups of $\mathbf{SL}(3)$. For each case, a hemisphere representation (left) and the corresponding planar image projection (right) are shown. Image points are grouped into orbits induced by the associated group action; all points in the same orbit share the same color (intensity). Selected orbits are highlighted in grayscale to emphasise the underlying symmetry structure.

Proof. This theorem can be proved using classical Lyapunov theory by choosing the candidate Lyapunov function $\mathcal{L}(E) := \mathcal{C}(E, \dot{I})$. Its time derivative is

$$\begin{aligned}
 \dot{\mathcal{L}}(E) &= \int_{\mathcal{X}} \left(I^e(\mathbf{x}) - \dot{I}(\mathbf{x}) \right) \frac{d}{dt} \boldsymbol{\mu}(E^{-1}, \dot{I})(\mathbf{x}) dV_g \\
 &= \int_{\mathcal{X}} r(\mathbf{x}) \frac{d}{dt} \dot{I} \circ \boldsymbol{\rho}_E(\mathbf{x}) dV_g \\
 &= \int_{\mathcal{X}} r(\mathbf{x}) \frac{d}{dt} \dot{I} \circ \boldsymbol{\rho}_{\mathbf{x}}(E) dV_g \\
 &= \int_{\mathcal{X}} r(\mathbf{x}) D(\dot{I} \circ \boldsymbol{\rho}_{\mathbf{x}})(E) [\Delta E] dV_g \\
 &= \int_{\mathcal{X}} r(\mathbf{x}) \tilde{D} I^e(\mathbf{x}) D \boldsymbol{\rho}_{\mathbf{x}}(I_3) [\Delta] dV_g.
 \end{aligned}$$

Then, using (16), we can write

$$\begin{aligned}
 \dot{\mathcal{L}}(E) &= - \int_{\mathcal{X}} r(\mathbf{x}) \tilde{\nabla} I^e(\mathbf{x})^\top \pi_{\mathbf{x}} \Delta \mathbf{x} dV_g \\
 &= - \int_{\mathcal{X}} \left\langle r(\mathbf{x}) \tilde{\nabla} I^e(\mathbf{x}), \Delta \mathbf{x} \right\rangle dV_g \\
 &= - \left\langle \int_{\mathcal{X}} r(\mathbf{x}) \tilde{\nabla} I^e(\mathbf{x}) \mathbf{x}^\top dV_g, \Delta \right\rangle.
 \end{aligned} \tag{22}$$

Finally, choosing the correction Δ as in (21) yields

$$\dot{\mathcal{L}}(E) = -\frac{1}{k_\Delta} |\Delta|^2 \leq 0. \tag{23}$$

Thus, the time derivative $\dot{\mathcal{L}}$ is negative semi-definite, and equal to zero when $\Delta = 0$. By the non-degeneracy assumption of Lemma 2, there exists an open neighbourhood of the global minimum I_3 in $\mathbf{SL}(3)$ where the cost has compact connected sub-level sets all containing I_3 and no other critical point of the cost since its Hessian at this point is positive definite. Let

$\mathfrak{B}^E \subseteq \mathbf{SL}(3)$ be the largest such sub-level set of the cost function on which $\mathcal{C}(E, \mathring{I})$ is proper with respect to E . From this, it follows that E is locally bounded. Since \mathcal{L} is non-increasing as a result of (23), one ensures that all solutions with initial condition $E(0) \in \mathfrak{B}^E$ remains in \mathfrak{B}^E for all time. The error dynamics (11) are autonomous, then by application of LaSalle's invariance principle [Khalil and Grizzle, 2002], we deduce that all solutions of this system with $E(0) \in \mathfrak{B}^E$ converge to the largest invariant set contained in $\mathcal{J} = \{E \in \mathfrak{B}^E : \Delta(E) = 0\}$. And since $\Delta(E) = 0$ (or equivalently $\nabla \mathcal{C}(E, \mathring{I}) = 0$) on \mathfrak{B}^E implies that $E = I_3$, it follows that the largest invariant subset of \mathcal{J} is $\{I_3\}$ and $E \rightarrow I_3$ for all $E(0) \in \mathfrak{B}^E$.

To conclude local exponential stability of the equilibrium $E = I_3$, we linearise the error dynamics about I_3 by writing $E \approx I_3 + \varepsilon^\wedge$, with normal coordinates $\varepsilon \in \mathbb{R}^8$. From (11), the first-order approximation of the error dynamics is $\dot{\varepsilon} = \Delta^\vee + \mathcal{O}(|\varepsilon|^2)$. The measurement residual is $\tilde{\mathbf{y}}(\varepsilon) := I^e - \mathring{I} \in \mathbb{L}^2(\mathcal{X})$. A first-order expansion about $\varepsilon = 0$ yields $\tilde{\mathbf{y}}(\varepsilon) = C\varepsilon + \mathcal{O}(|\varepsilon|^2)$, where $C : \mathbb{R}^8 \rightarrow \mathbb{L}^2(\mathcal{X})$ is the Jacobian operator of the warped image map evaluated at $E = I_3$, with conjugate $C^* : \mathbb{L}^2(\mathcal{X}) \rightarrow \mathbb{R}^8$. Since the cost function satisfies $\mathcal{C}(E, \mathring{I}) = \frac{1}{2} \|\tilde{\mathbf{y}}(E)\|^2$, its second-order expansion in normal coordinates is $\mathcal{C}(\varepsilon) = \frac{1}{2} \varepsilon^\top C^* C \varepsilon + \mathcal{O}(|\varepsilon|^3)$, which shows that $\text{Hess} \mathcal{C}(I_3, \mathring{I}) = C^* C$. By the non-degeneracy assumption of Lemma 2, $C^* C$ is positive definite. Since the correction Δ is chosen from the gradient of the cost, it satisfies in local coordinates $\Delta^\vee = -k_\Delta C^* C \varepsilon + \mathcal{O}(|\varepsilon|^2)$. The linearised error dynamics therefore reduce to $\dot{\varepsilon} = -k_\Delta C^* C \varepsilon$. Define the Lyapunov function $\mathcal{L}_{\text{lin}}(\varepsilon) := \frac{1}{2} |\varepsilon|^2$. Its time derivative along the linearised dynamics satisfies $\dot{\mathcal{L}}_{\text{lin}}(\varepsilon) = -k_\Delta \varepsilon^\top C^* C \varepsilon \leq -2k_\Delta \lambda_{\min} \mathcal{L}_{\text{lin}}(\varepsilon)$, where $\lambda_{\min} > 0$ denotes the smallest eigenvalue of $C^* C$. It follows that $\varepsilon \rightarrow 0$ exponentially, and therefore the equilibrium $E = I_3$ is locally exponentially stable. \square

4.1 Matrix-gain extension of the gradient observer

Using a scalar gain in the correction (21) ignores the underlying 8-dimensional geometry of $\mathfrak{sl}(3)$, and may limit convergence. In general, the scalar gain can be replaced by any 8×8 positive-definite matrix, which allows the gradient components to be scaled differently in the canonical coordinates of $\mathfrak{sl}(3)$. In particular, the gain can be chosen as the inverse of the Hessian of the cost function, which compensates for variations in the sensitivity of the cost along different directions. This extension is formalised in the following proposition.

Proposition 2. *Consider the homography kinematics (9) and observer (10). Consider the cost function defined by (14) and suppose that the cost is non-degenerate in the sense of Lemma 2. Define the correction by*

$$\Delta = \left(\mathbf{K} \left(\int_{\mathcal{X}} r(\mathbf{x}) \tilde{\nabla} I^e(\mathbf{x}) \mathbf{x}^\top dV_g \right)^\vee \right)^\wedge, \quad (24)$$

where $\mathbf{K} = k_\Delta (\text{Hess} \mathcal{C}(I_3, \mathring{I}))^{-1}$, where $\text{Hess} \mathcal{C}(I_3, \mathring{I})$ denotes the Hessian matrix of \mathcal{C} evaluated at I_3 given by

$$\text{Hess} \mathcal{C}(I_3, \mathring{I}) = \int_{\mathcal{X}} (\tilde{\nabla} \mathring{I}(\mathbf{x}) \mathbf{x}^\top)^\vee (\tilde{\nabla} \mathring{I}(\mathbf{x}) \mathbf{x}^\top)^\vee{}^\top dV_g. \quad (25)$$

Then, the observer dynamics (10) achieve local exponential convergence around the equilibrium $E = I_3$ with convergence rate k_Δ .

Proof. The Hessian of \mathcal{C} at I_3 is the symmetric matrix satisfying $D_1^2 \mathcal{C}(I_3, \mathring{I})[\Delta, \Delta] = \langle \Delta^\vee, \text{Hess} \mathcal{C} \Delta^\vee \rangle$. Using (17), the second-order derivative of \mathcal{C} at I_3 writes

$$\begin{aligned} D_1^2 \mathcal{C}(I_3, \mathring{I})[\Delta, \Delta] &= \int_{\mathcal{X}} \left\langle \tilde{\nabla} \mathring{I}(\mathbf{x}) \mathbf{x}^\top, \Delta \right\rangle^2 dV_g, \\ &= \int_{\mathcal{X}} \left\langle (\tilde{\nabla} \mathring{I}(\mathbf{x}) \mathbf{x}^\top)^\vee, \Delta^\vee \right\rangle^2 dV_g, \\ &= \left\langle \Delta^\vee, \int_{\mathcal{X}} \left((\tilde{\nabla} \mathring{I}(\mathbf{x}) \mathbf{x}^\top)^\vee (\tilde{\nabla} \mathring{I}(\mathbf{x}) \mathbf{x}^\top)^\vee{}^\top dV_g \right) \Delta^\vee \right\rangle. \end{aligned}$$

Then, direct identification yields expression (25). Now, consider the Lyapunov function $\mathcal{L}(E) := \mathcal{C}(E, \mathring{I})$. Using (11), recall that the time derivative of \mathcal{L} is given by

$$\dot{\mathcal{L}}(E) = - \left\langle \int_{\mathcal{X}} r(\mathbf{x}) \tilde{\nabla} I^e(\mathbf{x}) \mathbf{x}^\top dV_g, \Delta \right\rangle,$$

From the definition (24) of Δ and the properties of the vee-wedge operators, we have

$$\begin{aligned}\dot{\mathcal{L}}(E) &= -\left\langle (\mathbf{K}^{-1}\Delta^\vee)^\wedge, \Delta \right\rangle, \\ &= -\left\langle \mathbf{K}^{-1}\Delta^\vee, \Delta^\vee \right\rangle = -|\Delta^\vee|_{\mathbf{K}^{-1}}^2.\end{aligned}$$

The time derivative $\dot{\mathcal{L}}$ is negative semi-definite. Following the same steps as in the proof of Theorem 1 and using LaSalle's invariance principle, we show that E converges to the identity for all solutions with initial conditions $H(0) \in \mathbf{SL}(3)$ and $\dot{H}(0) \in \mathfrak{sl}(3)$ such that $E(0) \in \mathfrak{B}^E$.

To analyse the local convergence properties, consider the first-order approximation $E \approx I_3 + \varepsilon^\wedge$. Assuming that condition (19) holds and substituting the gain $\mathbf{K} = k_\Delta(C^*C)^{-1}$, the linearised error dynamics simplify to $\dot{\varepsilon} = -k_\Delta(C^*C)^{-1}C^*C\varepsilon = -k_\Delta\varepsilon$. Computing the time derivative of the Lyapunov function $\mathcal{L}_{\text{lin}}(\varepsilon) := \frac{1}{2}|\varepsilon|^2$ we get $\dot{\mathcal{L}}_{\text{lin}}(\varepsilon) = -k_\Delta|\varepsilon|^2 = -2k_\Delta\mathcal{L}_{\text{lin}}(\varepsilon)$. It follows that $\mathcal{L}_{\text{lin}}(\varepsilon)$ decreases exponentially and the error ε converges exponentially to zero at rate k_Δ . \square

Remark 4. Another specialisation of the gain $\mathbf{K} \in \mathbb{S}_+(8)$ exploits the decomposition of the $\mathfrak{sl}(3)$ algebra into orthogonal symmetric and skew-symmetric subspaces. Let $\mathbf{M} := \int_{\mathcal{X}} r(\mathbf{x})\tilde{\nabla}I^e(\mathbf{x})\mathbf{x}^\top d\mathbf{x} \in \mathfrak{sl}(3)$ and define the correction

$$\Delta = k_s\mathbb{P}_s(\mathbf{M}) + k_a\mathbb{P}_a(\mathbf{M}), \quad k_s, k_a > 0, \quad (26)$$

where the skew-symmetric subspace is the $\mathfrak{so}(3)$ algebra, and its orthogonal complement, the symmetric subspace of $\mathfrak{sl}(3)$, spans infinitesimal projective distortions (i.e., shearing and scaling). By tuning k_s and k_a , the observer can scale corrections along these subspaces and outperform (21) when homography errors are predominantly due to either projective deformations or rotations. Therefore, correction (26) offers an effective trade-off between computational efficiency and convergence performance.

5 Simulation results

In this section, we present the simulation experiment conducted to verify the performance and convergence of the proposed observer (10). From a reference image of a resolution of 256×254 pixels, the image at a given time was generated using $I = \mu(H, \dot{I})$. The true homography dynamics are defined according to (9), with initial condition and velocity

$$H(0) = \begin{pmatrix} 1.031 & 0.051 & 0.087 \\ -0.051 & 1.031 & -0.144 \\ 0 & 0 & 0.939 \end{pmatrix}, U(t) = \begin{pmatrix} 0 & 0 & -0.1 \\ 0 & 0 & 0.1 \\ 0 & 0 & 0 \end{pmatrix},$$

corresponding to a constant translational motion parallel to the plane, with angular velocity $\Omega(t) = 0$ and $\frac{d}{dt}(\xi/d) = (-0.1, 0.1, 0)^\top$.

The observer dynamics are defined according to (10) with initial condition $\hat{H}(0) = I_3$ and gain $k_\Delta = 0.01$. The true and estimated dynamics are integrated using Euler integration for 3 s with a time-step of 0.01 s using the matrix exponential to ensure that they remain in the Lie group $\mathbf{SL}(3)$ for all time. Due to discretisation errors, the numerical estimate may drift from $\mathbf{SL}(3)$ and is therefore re-projected onto the group using (3).

5.1 Results and discussion

The results are presented in Figures 3 and 4. Figure 3 reports the homography estimation error, $\epsilon_H = |I_3 - E|^2$, and the normalized image intensity error between the reference and warped images $\epsilon_I = \frac{1}{N}\|I^e - \dot{I}\|^2 = \frac{2}{N}\mathcal{C}(E, \dot{I})$, where N is the number of pixels. The performance of the scalar-gain correction (21) is compared with that obtained using the inverse Hessian-based correction term (24) and with the correction derived from the orthogonal decomposition described in Remark 4 with $k_s = k_\Delta$ and $k_a = 2k_\Delta$.

The results indicate that all three observers achieve convergence of both ϵ_H and ϵ_I to zero. The observer based on the orthogonal decomposition converges faster than the scalar-gain observer, while the inverse-Hessian-based observer achieves the fastest convergence, with the error decreasing exponentially. Note that the errors do not converge exactly to zero due to pixel mismatch at the image borders introduced by the warping function, which prevents perfect alignment of all pixels of the warped and reference images even when the observer has converged.

Figure 4 shows the evolution of the warped image and the corresponding difference image with respect to the reference at $t = 0$ s, $t = 0.15$ s, and $t = 1$ s. The results confirm that the warped image progressively converges to the reference image over time. The intensity-based observer (10) progressively aligns the warped image with the reference. The correction is driven by intensity differences within overlapping regions between I^e and \dot{I} . As the warped image converges toward the reference, the overlap error decreases, the magnitude of the correction diminishes, and the cost converges to zero.

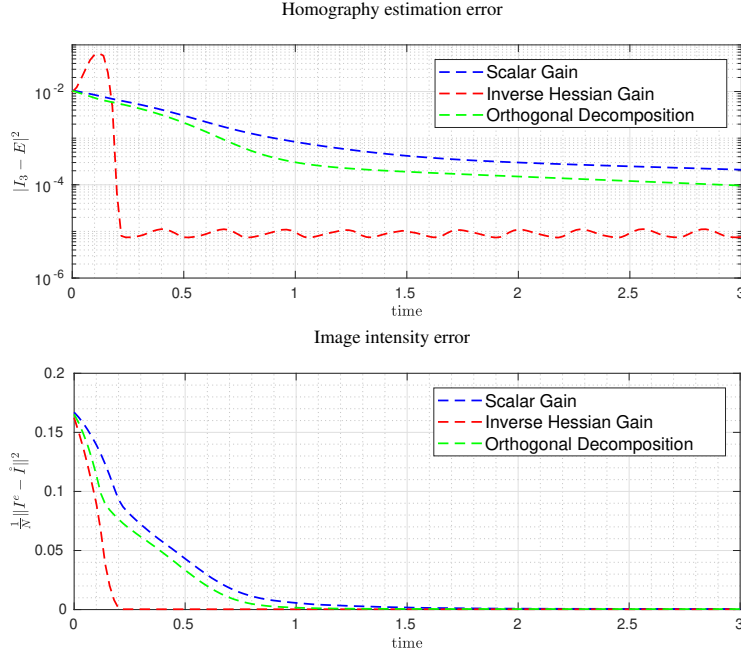


Figure 3: Time evolution of the homography estimation error (in semilogarithmic scale) and normalised image intensity error for the observer (10) using the single scalar gain (blue), the inverse Hessian gain (red) and the orthogonal decomposition dual-gain (green).

6 Conclusions

This work introduced a nonlinear observer framework for dynamic homography estimation from raw image intensities. By exploiting the $SL(3)$ Lie group structure and its induced action on the Sobolev space $W^{2,2}(\mathbb{S}^2)$, we defined a photometric cost function and derived a gradient-based observer. Local convergence was further improved through a matrix-gain formulation, in particular by incorporating the Hessian matrix. A detailed observability analysis established a local non-degeneracy condition and identified degenerate image configurations associated with invariance to $SL(3)$ subgroups. Simulation experiments on real image sequences confirmed convergence, robustness, and performance improvements of the proposed observers. This is the first direct, intensity-based nonlinear observer on $SL(3)$. The proposed dense framework could be in principle extended to other state estimation problems where the system evolves on a matrix Lie group and dense sensor measurements are available. A natural direction is the estimation of rigid-body motion on the Special Euclidean Group $SE(2)$ or $SE(3)$ using depth measurements.

Acknowledgment

This work was supported by the Grands Fonds Marins Project Deep-C, the ASTRID ANR project ASCAR (ANR-23-ASTR-0016), the European Union through the Horizon Europe Research and Innovation Programme (Grant Agreement No. 101154194, MEW), and the Australian Research Council through Discovery Grant DP250100112, “Seeing through Space and Time: Spatio-Temporal Event Processing for Robots”.

References

- Christian Forster, Matia Pizzoli, and Davide Scaramuzza. Svo: Fast semi-direct monocular visual odometry. In *2014 IEEE international conference on robotics and automation (ICRA)*, pages 15–22. IEEE, 2014.
- Andreas Geiger, Julius Ziegler, and Christoph Stiller. Stereoscan: Dense 3d reconstruction in real-time. In *2011 IEEE intelligent vehicles symposium (IV)*, pages 963–968. Ieee, 2011.
- Christian Kerl, Jürgen Sturm, and Daniel Cremers. Robust odometry estimation for rgb-d cameras. In *2013 IEEE international conference on robotics and automation*, pages 3748–3754. IEEE, 2013.
- Richard Hartley and Andrew Zisserman. *Multiple view geometry in computer vision*. Cambridge university press, 2003.

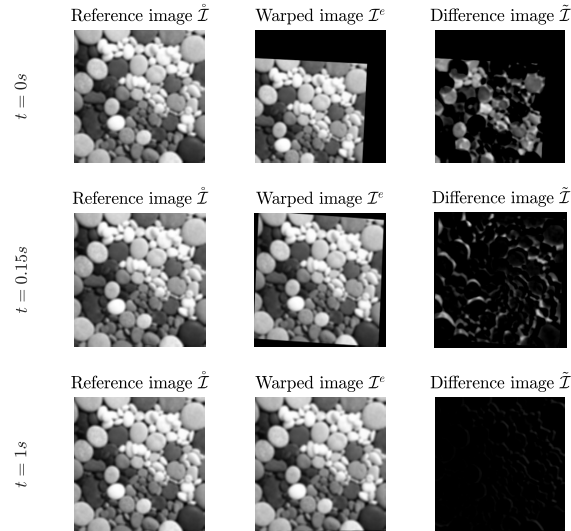


Figure 4: Reference image \tilde{I} , warped image I^e and difference image $\tilde{\tilde{I}}$ at selected time intervals, using the observer (10). As the observer converges, the warped image progressively aligns with the reference image, and correspondingly, the difference image approaches zero.

Jeremy Yermiyahou Kaminski and Amnon Shashua. Multiple view geometry of general algebraic curves. *International Journal of Computer Vision*, 56(3):195–219, 2004.

Anubhav Agarwal, CV Jawahar, and PJ Narayanan. A survey of planar homography estimation techniques. *Centre for Visual Information Technology, Tech. Rep. IIIT/TR/2005/12*, 2005.

Richard Szeliski et al. Image alignment and stitching: A tutorial. *Foundations and Trends® in Computer Graphics and Vision*, 2(1):1–104, 2007.

Heung-Yeung Shum and Richard Szeliski. Construction and refinement of panoramic mosaics with global and local alignment. In *Sixth International Conference on Computer Vision (IEEE Cat. No. 98CH36271)*, pages 953–956. IEEE, 1998.

Simon Baker and Iain Matthews. Lucas-kanade 20 years on: A unifying framework. *International journal of computer vision*, 56(3):221–255, 2004.

Selim Benhimane and Ezio Malis. Real-time image-based tracking of planes using efficient second-order minimization. In *2004 IEEE/RSJ International Conference on Intelligent Robots and Systems (IROS)(IEEE Cat. No. 04CH37566)*, volume 1, pages 943–948. IEEE, 2004.

Richard Szeliski and Sing Bing Kang. Direct methods for visual scene reconstruction. In *Proceedings IEEE Workshop on Representation of Visual Scenes (In Conjunction with ICCV’95)*, pages 26–33. IEEE, 1995.

Bruce D Lucas and Takeo Kanade. An iterative image registration technique with an application to stereo vision. In *IJCAI’81: 7th international joint conference on Artificial intelligence*, volume 2, pages 674–679, 1981.

Heung-Yeung Shum and Richard Szeliski. Construction of panoramic image mosaics with global and local alignment. *International Journal of Computer Vision*, 48(2):151–152, 2002.

Selim Benhimane and Ezio Malis. Homography-based 2d visual tracking and servoing. *The International Journal of Robotics Research*, 26(7):661–676, 2007.

Robert Mahony, Tarek Hamel, Pascal Morin, and Ezio Malis. Nonlinear complementary filters on the special linear group. *International Journal of Control*, 85(10):1557–1573, 2012.

Tarek Hamel, Robert Mahony, Jochen Trunpf, Pascal Morin, and Minh-Duc Hua. Homography estimation on the special linear group based on direct point correspondence. In *2011 50th IEEE Conference on Decision and Control and European Control Conference*, pages 7902–7908. IEEE, 2011.

Minh-Duc Hua, Jochen Trunpf, Tarek Hamel, Robert Mahony, and Pascal Morin. Feature-based recursive observer design for homography estimation and its application to image stabilization. *Asian Journal of Control*, 21(4):1443–1458, 2019.

Minh-Duc Hua, Jochen Trunpf, Tarek Hamel, Robert Mahony, and Pascal Morin. Nonlinear observer design on $sl(3)$ for homography estimation by exploiting point and line correspondences with application to image stabilization. *Automatica*, 115:108858, 2020.

- Robert Mahony, Jochen Trumpf, and Tarek Hamel. Observers for kinematic systems with symmetry. *IFAC Proceedings Volumes*, 46(23):617–633, 2013.
- Minh-Duc Hua, Tarek Hamel, Robert Mahony, and Guillaume Allibert. Explicit complementary observer design on special linear group $sl(3)$ for homography estimation using conic correspondences. In *2017 IEEE 56th Annual Conference on Decision and Control (CDC)*, pages 2434–2441. IEEE, 2017.
- Arturo Del Castillo Bernal, Philippe Decoste, and James Richard Forbes. Bayesian filtering for homography estimation. *IEEE Robotics and Automation Letters*, 2023.
- Tarek Bouazza, Katrina Ashton, Pieter van Goor, Robert Mahony, and Tarek Hamel. Equivariant filter for feature-based homography estimation for general camera motion. In *2023 62nd IEEE Conference on Decision and Control (CDC)*, pages 8463–8470. IEEE, 2023a.
- Tarek Bouazza, Pieter Van Goor, Robert Mahony, and Tarek Hamel. Nonlinear constructive observer design for direct homography estimation. *IFAC-PapersOnLine*, 56(2):1655–1660, 2023b.
- Chi Hin Chan and Magdalena Czubak. The meyers-serrin theorem on riemannian manifolds: a survey. *arXiv preprint arXiv:2405.13322*, 2024.
- Emmanuel Hebey. *Sobolev spaces on Riemannian manifolds*, volume 1635. Springer Science & Business Media, 1996.
- Andrew Baker. *Matrix groups: An introduction to Lie group theory*. Springer Science & Business Media, 2003.
- Yi Ma, Stefano Soatto, Jana Košecká, and Shankar Sastry. *An invitation to 3-d vision: from images to geometric models*, volume 26. Springer, 2004.
- Michal Irani and Prabu Anandan. About direct methods. In *International Workshop on Vision Algorithms*, pages 267–277. Springer, 1999.
- Hassan K Khalil and Jessy W Grizzle. *Nonlinear systems*, volume 3. Prentice hall Upper Saddle River, NJ, 2002.